Indian Journal of Chemistry
Vol. 64, January 2025, pp. 98-105
DOI: 10.56042/ijc.v64i1.15086

Synthesis of a redox-active pyrene-F_LF_L-dopamine amphiphile and investigation of their self-assembly at different *p*H leading to microfibrous formation

Shailesh S Birajdar[a,g], Kerba More[b], Prabhat K Singh[d,e], Avinash L Puyad[f], Mohammad Al Kobaisi[h], Sheshanath V Bhosale[c] & Sidhanath V Bhosale*[a,g]

[a] Polymers and Functional Materials Division, CSIR-Indian Institute of Chemical Technology, Hyderabad 500 007, Telangana, India

[b] School of Chemical Sciences, Goa University, Taleigao Plateau, Goa 403 206, India

[c] Department of Chemistry, School of Chemical Sciences, Central University of Karnataka, Kadaganchi, Kalaburagi 585 367, Karnataka, India

[d] Radiation and Photochemistry Division, Bhabha Atomic Research Centre, Mumbai 400 085, India

[e] Homi Bhabha National Institute, Training School Complex, Anushaktinagar, Mumbai 400 094, India

[f] School of Chemical Sciences, Swami Ramanand Teerth Marathwada University, Nanded 431 606, Maharashtra, India

[g] Academy of Scientific and Innovative Research (AcSIR), CSIR-HRDC Campus, Postal Staff College Area, Sector 19, Kamla Nehru Nagar, Ghaziabad 201 002, Uttar Pradesh, India

[h] School of Science, RMIT University, GPO Box 2476, Melbourne, VIC, 3001, Australia

E-mail: bhosale@iict.res.in, bsheshanath@cuk.ac.in

Received 14 November 2024; accepted (revised) 27 December 2024

N-(1-((1-((3,4-Dihydroxyphenethyl)amino)-1-oxo-3-phenylpropan-2-yl)amino)-1-oxo-3-phenylpropan-2-yl)-4-(pyren-1-yl)butanamide (Py-F_L-F_L-DP) has been synthesised using the traditional amide coupling reactions of 1-pyrene butyric acid, boc-l-phenyl alanine, l-phenyl alanine methyl ester and dopamine. Py-F_L-F_L-DP shows a *p*H dependant aggregation between *p*H 4 and 10 which can be monitored spectroscopically, resulting in a reversible quinone/hydroquinone oxidation – reduction transformation of the dopamine moiety. The photoexcitation of Py-F_L-F_L-DP at λ_{ex} 345 nm at higher *p*H preferentially results in aggregation induced emission (AIE) photorelaxation mechanism in comparison to thermal relaxation or intramolecular charge transfer (ICT). SEM micrographs show the formation of fibrillar nanostructure with increasing *p*H specially at *p*H 10. The CD experiment offers deeper insights into the chirality that developed in the nanofiber self-assemblies at *p*H levels 7 to 10, which is attributed to the twisted conformations of the pyrene moieties within the self-assembled structure. The unique *p*H-dependent self-assembly and redox behavior of Py-F_L-F_L-DP, particularly its reversible optical and structural changes in response to *p*H variations, make it a promising candidate for real-time *p*H monitoring in biomedical applications, such as intracellular imaging and the design of controlled drug delivery systems targeting *p*H-sensitive environments.

Keywords: Pyrene, Dopamine, L-Phenylalanine, UV-Vis, Emission, Self-assembly

Intracellular *p*H plays an important role in regulating various cellular processes, such as pathological and physiological and the function of different organelles, enzymes and degradation of proteins[1,2]. Intracellular *p*H value in mammalian cells is ranging from 4.7 in lysosome to 8.0 in mitochondria[3,4]. The variation of intracellular *p*H from its ideal value may cause organelle functional disorder, leading to various diseases, such as strokes, Alzheimer's and cancers[5-7]. The development of organic fluorescence molecular architecture for measuring intracellular *p*H from acidic to alkaline range is in urgent demand. Recent studies on *p*H-sensitive amphiphilic molecules have focused on designing systems that respond to environmental changes with high sensitivity and stability, especially across a broad *p*H spectrum. For instance, several pyrene-based amphiphilic probes have shown promise for intracellular *p*H monitoring due to their fluorescence properties and structural adaptability. However, many existing probes are limited by either a narrow *p*H response range or instability in biologically relevant conditions, which can reduce their applicability in real-time monitoring of *p*H fluctuations in diverse cellular environments.

Here, we developed a simple and effective donor-linker-acceptor molecular architecture based on pyrene (Py)-L,L-diphenylalanine (F_LF_L)-dopamine

(DP) conjugate to be used as photophysical probe (Scheme 1). Pyrene[8] as a donor provides fluorescence in the visible range, excimer formation, and long-lived excited states with high quantum yield[9]. Pyrene also displays outstanding cell permeability[10] and has been employed in biological live cell imaging[11]. The F_LF_L dipeptide undergoes self-assembly leading to formation of supramolecular nanostructures having various potential bio-applications[12]. Dopamine is a neurotransmitter with key roles in the central nervous system, renal systems, hormonal systems, cardiovascular systems and Parkinson's disease[13]. Dopamine shows redox properties at different *p*H (Ref. 14). The redox behaviour of dopamine in combination with cationic polymers (CPs) and malachite green cabinol base can form *p*H responsive complex that can be used in sensing applications in aqueous media[15]. Recently, dopamine functionalized donor-acceptor polymer was used to detect *p*H in living cell lines and autophagy imaging[16].

The Py-F_L-F_L-DP chromophore developed in this study offers several advantages over traditional probes. Its molecular design, combining the redox-active dopamine with a Py-F_L-F_L framework, not only provides stability over an extended *p*H range (3 to 11) but also exhibits reversible optical changes due to the redox properties of dopamine. This extended *p*H sensitivity, coupled with its enhanced self-assembly properties driven by the F_LF_L dipeptide, enables Py-F_L-F_L-DP to maintain functional performance even under varied *p*H conditions. Furthermore, the unique donor-acceptor structure of Py-F_L-F_L-DP supports both aggregation-induced emission (AIE) and intramolecular charge transfer (ICT), optimizing it for dual-mode sensing, which is less common among currently available *p*H-sensitive amphiphiles.

Inspired by the importance of Py, F_LF_L and DP in biological applications, we present the design strategy, synthesis, and spectroscopic characterization of Py-F_L-F_L-DP chromophore (Scheme 1). Here we study the experimental *p*H response in UV-vis absorbance and fluorescence emission of Py-F_L-F_L-DP, as well as the theoretical molecular modelling of this chromophore. Thus, this study provides a novel, *p*H-responsive chromophore with a broader *p*H sensitivity and improved stability, positioning Py-F_L-F_L-DP as a versatile candidate for applications in dynamic *p*H monitoring, particularly in intracellular imaging and potential therapeutic delivery systems.

Experimental Section

Synthesis of methyl (tert-butoxycarbonyl) phenylalanylphenylalaninate, 3

In a 25 mL round bottomed flask compound boc-l-phenyl alanine **1** (0.265 mg, 1mmol), EDC HCl (230 mg, 1.2 mmol) was added to 15 mL dry DMF under nitrogen atmospheric condition. Stirred the reaction mixture for half an hour at 0°C. The l-phenyl alanine methyl ester **2** (215 mg, 1 mmol) and DIPEA (155 mg, 1.2 mmol) were added to the reaction mixture at RT. The above reaction mixture allowed to stir for a 24 h at RT. After completion of reaction (monitored by using TLC), solvent was removed with rotary evaporation. The reaction mixture was eluted using 50 mL of ethyl acetate and sequentially washed with 10% w/v $NaHCO_3$ solution (2×30 mL), 0.1 M HCl (20 mL), followed by rinses with water (20 mL) and brine (20 mL). The organic phase was then dried over anhydrous sodium sulfate, filtered, and concentrated under reduced pressure. The resulting residue was purified by flash chromatography on silica gel (SiO_2), using a 1% methanol in chloroform eluent, yielding compound 3 as a white powder. (395 mg, 80%). ^{1}H NMR (300 MHz, $CDCl_3$): δ 7.30-7.27 (m, 2H), 7.24-7.22 (m, 4H), 7.16-7.15 (d, 2H), 6.94-6.93 (d, 2H), 6.41 (s, 1H), 4.95-4.97 (m, 1H), 4.84-4.80 (m, 1H), 4.36 (s, 1H), 3.66 (s, 3H), 3.08-2.92 (m, 4H), 1.38 (s, 9H); ^{13}C NMR ($CDCl_3$, 75 MHz): δ 171.29, 170.85, 155.19, 136.43, 135.58, 129.26, 129.13, 128.53, 128.44, 127.00, 126.85, 80.18, 55.63, 53.22, 52.15, 38.19, 37.88, 28.14; ESI-MS: *m/z* Calcd for $C_{22}H_{30}N_2O_5$: 426.50. Found: 427 $[M+H]^+$.

Synthesis of methyl (4-(pyren-1-yl)butanoyl) phenylalanylphenylalaninate, 5

In a 25 mL round bottomed flask having 8:6 mL dry DCM: TFA under nitrogen atmospheric condition methyl (*tert*-butoxycarbonyl)-L-phenylalanyl-L-

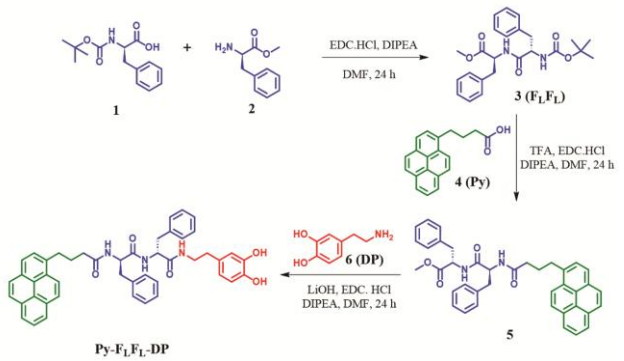

Scheme 1 — Synthetic route for Py-F_L-F_L-DP chromophore

phenylalaninate (**3)** (223 mg, 0.5 mmol) was added. The above reaction mixture was allowed to be stirred for 2 h. After completion of reaction (monitored by using TLC), solvent was removed with rotary evaporation. The white solid product was dried under vacuum. To a 25 mL round-bottom flask containing a solution of 1-pyrene butyric acid **4** (144 mg, 0.25 mmol) in 10 mL of dry DMF under a nitrogen atmosphere, EDC·HCl (48 mg, 0.25 mmol) was added. The above reaction was stirred for half an h at 0°C. The Boc deprotected diphenyl alanine methyl ester hydrochloride salt (126.50 mg, 0.25 mmol) and DIPEA (0.33 mg, 0.25 mmol) were added to the reaction mixture. The above reaction mixture was stirred for 24 h. After completion of reaction (monitored by using TLC), the solvent was removed with rotary evaporation. The reaction mixture was eluted with 50 mL of ethyl acetate and washed sequentially with 10% w/v $NaHCO_3$ solution (2×10 mL), 0.1 M HCl (2×20 mL), followed by 20 mL of water and 20 mL of brine. The organic layer was then dried over anhydrous sodium sulfate, filtered, and concentrated under reduced pressure. The residue was purified by flash silica gel chromatography (SiO_2) by eluting with 1% methanol: chloroform solution to give **5** as white powder (181 mg, 70%). ^{1}H NMR (300 MHz, $CDCl_3$): δ 8.26-8.24 (d, 1H), 8.17-8.15 (m, 2H), 8.11-8.09 (m, 2H), 8.09-8.03 (d, 2H), 8.00-7.97 (m, 1H), 7.80-7.78 (d, 1H), 7.24-7.22 (d, 2H), 7.19-7.09 (m, 6H), 6.97-6.96 (m, 2H), 6.17-6.15 (d, 1H), 5.95-5.93 (d, 1H), 4.75-4.71 (m, 1H), 4.68-4.64 (m, 1H), 3.66 (s, 3H), 3.31-3.28 (t, 2H), 3.09-2.93 (m, 4H), 2.26-2.23 (m, 2H), 2.15-2.10 (m, 2H); ^{13}C NMR ($CDCl_3$, 75 MHz): δ 172.54, 171.37, 170.49, 136.36, 135.39, 131.36, 130.85, 129.91, 129.52, 129.25, 129.09, 128.67, 128.58, 127.44, 127.36, 127.31, 127.17, 127.08, 126.68, 125.80, 125.03, 124.93, 124.87, 124.74, 123.31, 54.23, 53.40, 53.02, 52.29, 38.20, 37.76, 35.80, 32.61, 29.68, 27.13; ESI-MS: *m/z* Calcd for $C_{40}H_{38}N_2O_5$: 596.71. Found: 597 $[M+H]^+$.

Synthesis of N-(1-((1-((3,4-dihydroxyphenethyl) amino)-1-oxo-3-phenylpropan-2-yl)amino)-1-oxo-3-phenylpropan-2-yl)-4-(pyren-1-yl)butanamide [Py-F_LF_L-DP]

In a 25 mL round bottomed flask compound **5** (178 mg, 0.3 mmol) was taken in 8:2 mL THF:MeOH solution. The above reaction mixture was allowed to stirred for 12 h at r.t. After completion of reaction (monitored by using TLC), the solvent was removed with rotary evaporation. The crude products were acidified with 0.1 N HCl, adjust the *p*H up to 2 and eluted with ethyl acetate (50 mL). The resultant organic solvent was dried over anhydrous sodium sulphate, filtered and reduced *in vacuo*. The above acid was used for further reaction without purification. To the solution of above acid (116 mg, 0.2 mmol) in dry DMF, 10 mL in 25 mL of round bottom flask under nitrogen atmosphere EDC. HCl (48 mg, 0.25 mmol) was added. The above reaction stirred for half an hour at 0°C. The dopamine (23.50 mg, 0.2 mmol) and DIPEA (0.33 mg, 0.25 mmol) were added to the reaction mixture. The above reaction mixture was stirred for 24 h. After completion of the reaction (monitored by using TLC), the solvent was removed with rotary evaporation. The reaction mixture was eluted with 50 mL of ethyl acetate, then washed with 10% w/v $NaHCO_3$ solution (2×10 mL), 0.1 M HCl (2×20 mL), followed by 20 mL each of water and brine. The organic layer was dried over anhydrous sodium sulfate, filtered, and concentrated under reduced pressure. The resulting residue was purified by flash chromatography on silica gel (SiO_2), using 1% methanol in chloroform as the eluent, yielding Py-FLFL-DP as a white powder. Yield 112 mg (80%). ^{1}H NMR (300 MHz, $CDCl_3$): δ 8.27-8.23 (m,1H), 8.17-8.15 (m, 2H), 8.11-8.07 (m, 2H), 8.11-8.07 (m, 2H), 8.03-8.02 (m, 2H), 7.96-8.00 (m, 1H), 7.81-7.79 (d, 1H), 7.62-7.59 (d, 1H), 7.46-7.43 (m, 1H), 7.34-7.31 (d, 1H), 7.22-7.08 (m, 10), 6.73-6.69 (m, 1H). 6.64-6.62 (d, 1H), 6.45-6.42 (d, 1H), 4.66-4.54 (m, 2H), 3.37-3.33 (m, 2H), 3.28-3.23 (m, 2H), 3.09-2.94 (m, 4H), 2.59-2.58 (t, 2H), 2.26-2.21 (m, 2H), 2.07-2.03 (m, 2H); ^{13}C NMR (300 MHz, $CDCl_3$): δ 172.35, 170.74, 169.98, 169.71, 143.92, 142.56, 136.52, 136.42, 135.37, 130.37, 129.91, 128.45, 128.34, 127.39, 126.61, 126.37, 125.69, 125.05, 123.96, 123.87, 122.66, 119.05, 114.71, 53.48, 46.98, 36.73, 34.66, 33.87, 31.80, 28.63, 26.49, 24.61; ESI-MS: *m/z* Calcd for $C_{46}H_{43}N_3O_5$: 717.85. Found: $[M+H]^+$ 718; HRMS (ESI): *m/z* Calcd for $C_{46}H_{43}N_3O_5$: 718.3275. Found: 718.3282.

Results and Discussion

Synthesis of Py-F_LF_L-DP

The synthetic route for Py-F_L-F_L-DP chromophore is outlined in Scheme 1, boc-l-phenyl alanine **1** was reacted with l-phenyl alanine methyl ester **2** in the presence of EDC.HCl to afford F_LF_L (**3**). Further, F_LF_L (**3**) was reacted with 1-pyrene butyric acid, Py

(**4**), to yield Py-F_LF_L (**5**) *via* an amide coupling reaction. Py-F_LF_L (**5**) methyl ester was first treated with lithium hydroxide to yield Py-F_LF_L (**5**) carboxylic acid. The Py-F_LF_L (**5**) carboxylic acid is further conjugated with dopamine in the presence of EDC.HCl in dimethylformamide at RT to yield Py-F_L-F_L-DP.

Photophysical properties of Py-F_L-F_L-DP

The photophysical properties of Py-FL-FL-DP were investigated at various *p*H's. Py-F_L-F_L-DP was soluble in a mixture of DMSO: H_2O (40:60, v/v ratio). Py-F_L-F_L-DP in DMSO:H_2O (40:60, v/v ratio) at *p*H 7 exhibited five absorption peaks at 267 nm (ε = 57000 M^{-1} cm^{-1}), 278 nm (ε = 86300 M^{-1} cm^{-1}), 315 nm (ε = 21700 M^{-1} cm^{-1}), 330 nm (ε = 44900 M^{-1} cm^{-1}) and 345 nm (ε = 58700 M^{-1} cm^{-1}) (Fig. 1a). The *p*H of the Py-F_L-F_L-DP solution in DMSO:H_2O was varied in the acidic range using 0.1 M HCl from 7 to 4, and in the basic range from *p*H 7 to 10 using 0.1 M NaOH. As we moved from lower *p*H 4 to higher *p*H 10, we observed that all absorbance values were increased, due to Mie scattering caused by particle formation in the solution, suggesting that Py-F_L-F_L-DP undergoes aggregation (Fig. 1a). To gain a clearer view of the sensitivity of Py-F_L-F_L-DP towards *p*H, we quantified the relative changes in absorbance and emission intensities across the *p*H range. At *p*H 4, the absorbance at 345 nm was observed to be approximately 25% lower than at *p*H 10, which aligns with the aggregation behavior indicated by Mie scattering effects in the higher *p*H range (Fig. 1a). Additionally, the absorption intensity increase from *p*H 4 to *p*H 10 was most pronounced for the peak at 278 nm, showing a rise of roughly 40% (Fig. 2a), further suggesting enhanced aggregate formation with increasing *p*H. Thus, the absorption spectroscopy indicates that the aggregation of Py-F_L-F_L-DP with changing *p*H (Fig. 2a).

The emission spectroscopy study of Py-F_L-F_L-DP was conducted under the same conditions as the absorbance experiment, with photoexcitation at 345 nm. The emission spectra of Py-F_L-F_L-DP in DMSO: H_2O (40:60, v/v ratio) at *p*H 7 displayed three significant peaks at 378, 399 and 419 nm. The influence of *p*H on the emission properties were investigated by varying *p*H ranging from 4 to 10. In the emission spectra, the fluorescence intensity at 399 nm was significantly enhanced by over 50% as *p*H increased from 4 to 10 (Fig. 1b). At higher *p*H, the fluorescence intensity of Py-F_L-F_L-DP increases

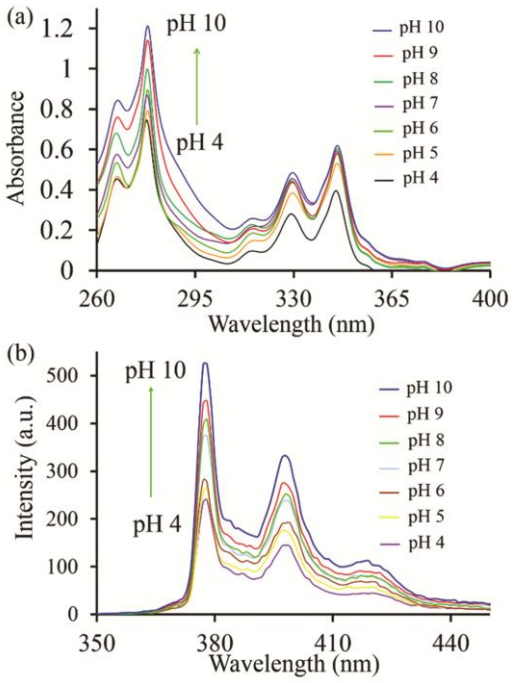

Fig. 1 — (a) UV-Vis absorption spectra of Py-F_L-F_L-DP (1×10^{-5} M) and (b) fluorescence emission spectra of Py-F_L-F_L-DP (1×10^{-5} M) at various *p*H in DMSO:H_2O (40:60, v/v ratio) solvent mixture (λ_{ex} = 345 nm)

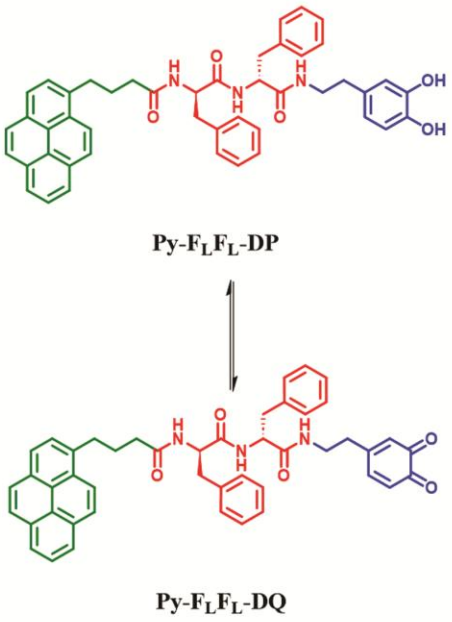

Fig. 2 — Py-F_L-F_L-DP in its reduced (*p*H < 7) *i.e.* hydroquinone and oxidized (*p*H > 7) quinone states

predominantly due to the aggregation-induced emission (AIE) mechanism, which appears to overshadow the intramolecular charge transfer (ICT) quenching effects that might otherwise reduce

emission intensity. Notably, the balance between AIE and ICT mechanisms shifted visibly around *p*H 7, where the emission intensities started to rise more sharply, suggesting a threshold *p*H that initiates prominent AIE behavior. This dominance of AIE at basic *p*H can be attributed to enhanced intermolecular interactions, particularly π-π stacking between the pyrene moieties, which become more favorable as *p*H increases and induces aggregation. These interactions facilitate the formation of emissive aggregates, which limit non-radiative decay pathways, thereby enhancing overall emission intensity.

In contrast, ICT effects, which typically lead to charge separation and reduce fluorescence, are mitigated at higher *p*H due to the oxidative state of the dopamine subunit. The oxidation of dopamine to quinone at elevated *p*H levels disrupts the electron-donating capacity of the dopamine unit, thereby reducing ICT efficiency. This allows AIE to become the primary contributor to emission. Studies on similar pyrene-based systems have shown that AIE effects are particularly robust in molecules with donor-acceptor configurations where the acceptor (here, dopamine) can undergo oxidation, thus weakening ICT pathways and favouring emission through aggregate formation[17].

The interplay between AIE and ICT in Py-F_L-F_L-DP demonstrates the molecule's sensitivity to *p*H-induced changes in its electronic structure, highlighting the potential of *p*H as a tunable factor for emission modulation in bioimaging and sensing applications. The observed dominance of AIE over ICT at basic *p*H aligns well with previous findings in similar amphiphilic systems, where AIE emerges as the primary emission pathway under conditions favouring molecular aggregation[18].

Theoretical *in vacuo* density functional theory (DFT) and time-dependent DFT (TD-DFT) simulations were carried out using the Gaussian 16 software package[19]. The geometry optimization and frequency calculations of Py-F_L-F_L-DP and Py-F_L-F_L-DP have been performed at B3LYP/6-31G* level of theory to confirm the structure energy minima. The obtained Py-F_L-F_L-DP and Py-F_L-F_L-DP geometries were subject to further TD-DFT simulation at B3LYP/6-31G* level of theory. TD-DFT results were analysed by employing Gauss-Sum 2.2.5 program (Table S1)[20]. From the TD-DFT results it is seen that absorption of Py-F_L-F_L-DP is at 341.23, 269.44, 269.19 nm and Py-F_L-F_L-DQ is at 408.91, 367.00, 341.22 nm. The frontier molecular orbitals (FMO) are generated by using Avogadro and are given in Fig. 3[21,22].

The DFT calculations reveal significant differences in the HOMO and LUMO energy levels and energy gaps (E_g) for Py-F_L-F_L-DP and its oxidized form, Py-F_L-F_L-DQ, which correspond to the redox behaviour of the molecule. For Py-F_L-F_L-DP, the HOMO energy level is calculated at -5.213 eV, and the LUMO at -1.444 eV, resulting in an energy gap of 3.769 eV. In this reduced hydroquinone state, the higher energy gap suggests limited electron mobility, which corresponds with the stable fluorescence emission observed in its reduced form at lower *p*H levels. Upon oxidation to Py-F_L-F_L-DQ, the HOMO drops slightly to -5.274 eV, while the LUMO decreases substantially to -3.415 eV, reducing the energy gap to 1.859 eV. The narrowing of the energy gap reflects the molecule's enhanced electron-accepting ability in the oxidized quinone state, thereby diminishing the ICT process and reducing non-radiative decay. Additionally, the localization of the HOMO on the dopamine moiety in both states supports the role of dopamine as an electron donor. In the reduced Py-F_L-F_L-DP form, electron-rich dopamine facilitates ICT, leading to partial quenching of fluorescence. However, in the oxidized Py-F_L-F_L-DQ form, the reduced electron-donating capacity of dopamine minimizes ICT effects, allowing AIE to become the predominant emission pathway. The theoretical calculations thus provide a clear mechanistic basis for the observed *p*H-dependent redox behavior and fluorescence modulation, reinforcing the suitability of Py-F_L-F_L-DP as a *p*H-sensitive probe.

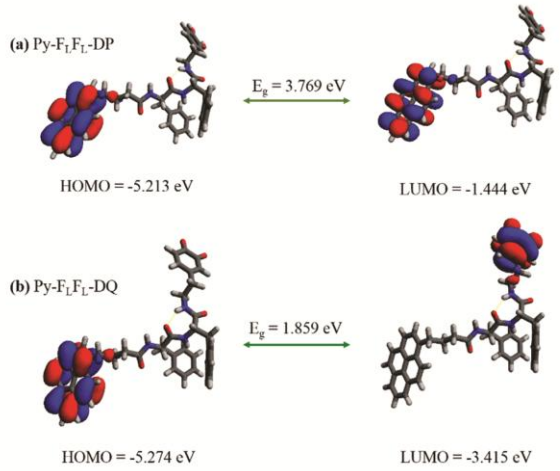

Fig. 3 — Frontier molecular orbitals of Py-F_L-F_L-DP and Py-F_L-F_L-DP energy levels and electron density as calculated at B3LYP/6-31G* level of theory

Scanning Electron Microscopy Study

The self-assembly of Py-F_L-F_L-DP was studied by depositing its DMSO-H_2O solution (40:60, v/v) at *p*H 4, 7, and 9.2 on silicon wafer substrates. The resulting morphology and microstructures were visualized using scanning electron microscopy (SEM). Microfibrous morphology was observed for Py-F_L-F_L-DP at all the studied *p*H's, *i.e.* 4.0, 7.0, and 9.2 (Fig. 4a,b,c). The SEM analysis of Py-F_L-F_L-DP self-assembly across different *p*H levels provides a clear view of the *p*H-dependent fiber morphology changes. At *p*H 4.0, the average fiber diameter was measured at approximately 17±3 nm, while at *p*H 9.2, this diameter increased to 21±6 nm, suggesting a consistent growth in fiber thickness with rising *p*H levels (Fig. 4d). This trend likely results from enhanced hydrophobic interactions and π-π stacking between the pyrene moieties as the dopamine subunit undergoes oxidation, converting hydroquinone to quinone and thereby increasing the rigidity and aggregation propensity of the fibers. At higher *p*H's, the hydroquinone of the dopamine subunit transforms to quinone. The hydroxyl groups in the hydroquinone moiety convert to ketone at a higher *p*H, increasing the possibility of hydrophobic interactions and therefore increasing the diameter of the microfibers self-assembled at higher *p*H's.

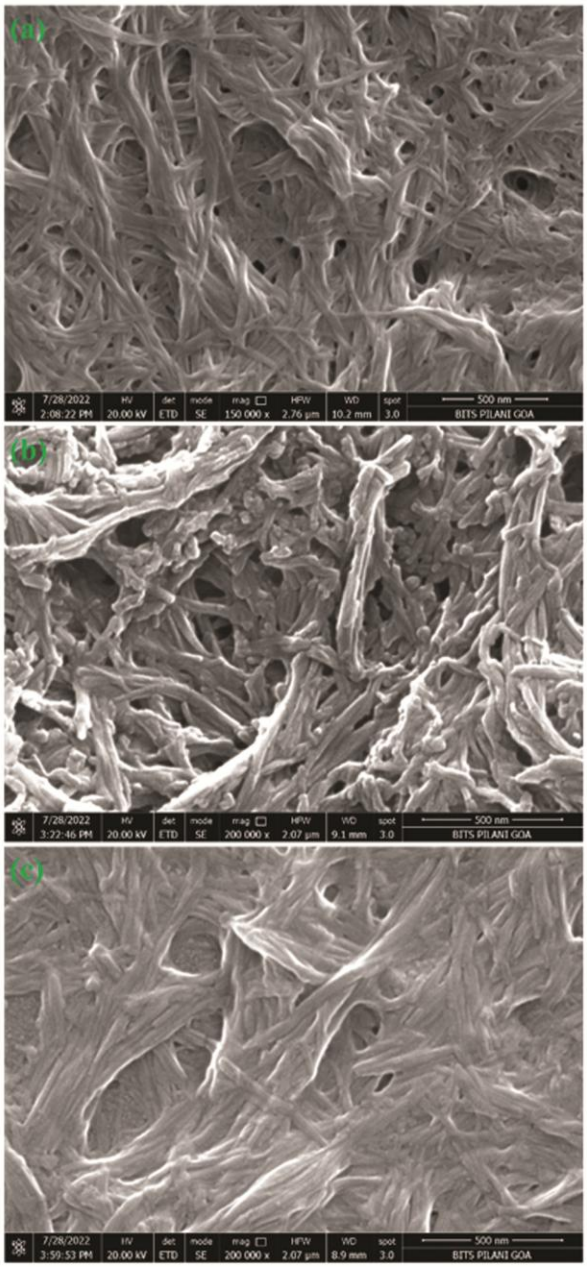

Fig. 4 — SEM micrographs of Py-F_L-F_L-DP self-assembled in DMSO:H_2O (40:60, v/v ratio) at *p*H's (a) 4.0, (b) 7.0 and (c) 9.2

Circular Dichroism Study

The CD spectra of Py-F_L-F_L-DP show distinct chiral signals at *p*H 7 and 10, indicative of the self-assembly's chiral arrangements in basic conditions, while negligible signals were observed at *p*H 4, where the molecule forms microcrystalline deposits (Fig. 5). At higher *p*H levels, quantitative analysis of the CD spectral features reveals an increase in ellipticity, particularly at wavelengths corresponding to the pyrene absorption regions. For instance, the ellipticity at 340 nm, which reflects the stacking interactions of pyrene units, shows a significant increase from *p*H 7 to *p*H 10. This *p*H-dependent enhancement of CD signals suggests stronger chiral arrangements and more defined twisting of the stacked pyrene units under basic conditions.

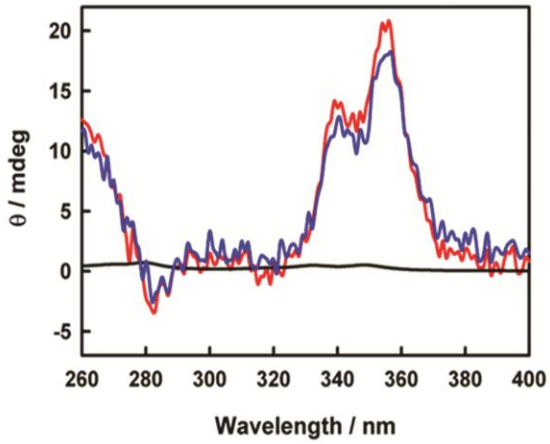

Fig. 5 — CD spectra of Py-F_L-F_L-DP in DMSO:H_2O (40:60, v/v ratio) at different *p*H 4 (black line); *p*H 7 (blue line) and *p*H 10 (red line)

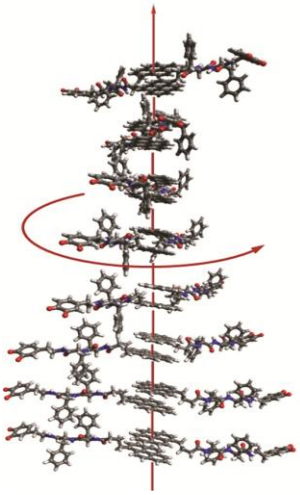

Fig. 6 — Self-assembly model of Py-F_L-F_L-DP forming nanofibers at high *p*H, with a characteristic twist that produces the observed CD signal

Furthermore, environmental factors, particularly *p*H, play a significant role in the observed CD signal variations. At higher *p*H, the transformation of dopamine from hydroquinone to quinone increases hydrophobic interactions and π-π stacking, leading to a more rigid, chiral self-assembly. In contrast, at *p*H 4, the molecule's reduced state favors a less ordered structure with minimal chirality, as evidenced by the absence of strong CD signals. At high *p*H, the self-assembly likely involves hydrophobic interactions between the central pyrene units, along with interactions between the F_L-F_L peptide moieties through their aromatic phenyl rings. The quinone groups are positioned on the periphery, where they interact with the surrounding solvent. This self-assembly exhibits a twist around the stacked pyrene units, which is evidenced by the chirality observed in the CD spectra (Fig. 6).

Schematic presentation of self-assembly process

Conclusions

In summary, we have successfully designed and synthesized Py-F_L-F_L-DP through standard amide coupling of pyrene butyric acid, protected phenylalanine, and dopamine derivatives. The molecule exhibits distinct redox properties in the dopamine motif, observed across the *p*H spectrum from 4 to 10 in absorption and emission experiments, and demonstrates aggregation behavior in response to *p*H changes. The findings indicate that the aggregation-induced emission (AIE) mechanism predominates over intramolecular charge transfer (ICT), significantly enhancing fluorescence emission at higher *p*H levels. The CD study and SEM images reveal that quinone formation in the dopamine subunit at higher *p*H promotes the formation of fibrillar nanostructures, especially at *p*H 10, and results in distinct chiral arrangements, likely due to twisted pyrene moieties. These *p*H-sensitive self-assembly and optical properties suggest that Py-F_L-F_L-DP has potential applications in biosensing, where it could serve as a fluorescent probe for monitoring *p*H variations in biological systems.

Supplementary Information

Supplementary information is available in the website http://nopr.niscpr.res.in/handle/123456789/58776.

Acknowledgements

Sidhanath V. B. (CSIR-IICT) is grateful for financial support from the Director, CSIR-IICT (MS No. IICT/Pubs./2024/406). Sheshanath V. B. acknowledges UGC-FRP for financial support and Professorship.

References

1 Kim D, Kim S, Park G, Choi H & Ryu J H, *JACS Au*, 2 (2022) 2539.
2 Olsnes S, Toennessen T I, Ludt J & Sandvig K, *Biochemistry*, 26 (1987) 2775.
3 Medintz I L, Stewart M H, Tramme S A, Susumu K, Delehanty J B, Mei B C, Melinger J S, Blanco-Canosa J B, Dawson P E & Mattoussi H, *Nat Mater*, 9 (2010) 676.
4 Ghosh G, Kartha K K & Fernández G, *Chem Commun.* 57 (2021) 1603.
5 Zheng X S, Zong C, Wang X & Ren B, *Anal Chem*, 91 (2019) 8383.
6 Mandell A J, Selz K A, Owens M J, Kinkead B, Shlesinger M F, Gutman D A & Arguragi V, *Neuropsychopharmacol.*, 28 (2003) S98.
7 Bobe, S R, Kobaisi M A, Bhosale S V & Bhosale S V, *ChemistryOpen*, 14 (2015) 516
8 Gil A M, Casanovas J, Mayans E, Jimenez A I, Puiggalí J & Alemań C, *J Phys Chem B*, 124 (2020) 5913.
9 Shete S, Gavali M, Ramana M M V, Maduskar M, Karanjule N & Yadav D K, *Indian J Chem*, 62 (2023) 1147.
10 Takeuchi T, Kosuge M, Tadokoro A, Sugiura Y, Nishi M, Kawata M, Sakai N, Matile S & Futaki S, *ACS Chem Biol* 1 (2006) 299.
11 Zhang L, Yang L, He Y & Han J M, *J Mater Chem A*, 10 (2022) 18363.
12 Padhi D, Balachandra C, Ramesh M & Govindaraju T, *Chem Comm*, 58 (2022) 6288.
13 Li Z, Zhu Y & Matson J B, *ACS Applied Bio Materials*, 5 (2022) 4635.
14 Argitekin E, Ersoz-Gulseven E, Cakan-Akdogan G & Akdogan Y, *Biomacromolecules*, 24 (2023) 3603.
15 Umek N, Geršak B, Vintar N, Šoštarič M & Mavri, J, *Front Mol Neurosci*, 11 (2018) 467.

16 Herrera A, Muñoz P, Steinbusch H W M, Segura-Aguilar J, *ACS Chem Neurosci*, 8 (2017) 702.
17 Hong Y, Lam J W Y & Tang B Z, *Chem Commun*, (2009) 4332-4353
18 Yuan J, Dong S & Hao J. *Curr Opin Colloid Interface Sci*, 63 (2023) 101657.
19 Gaussian 16, Revision B.01, Frisch M J, Trucks G W, Schlegel H B, Scuseria G E, Robb M A, Cheeseman J R, Scalmani G, Barone V, Petersson G A, Nakatsuji H, Li X, Caricato M, Marenich A V, Bloino J, Janesko B G, Gomperts R, Mennucci B, Hratchian H P, Ortiz J V, Izmaylov A F, Sonnenberg J L, Williams-Young D, Ding F, Lipparini F, Egidi F, Goings J, Peng B, Petrone A, Henderson T, Ranasinghe D, Zakrzewski V G, Gao J, Rega N, Zheng G, Liang W, Hada M, Ehara M, Toyota K, Fukuda R, Hasegawa J, Ishida M, Nakajima T, Honda Y, Kitao O, Nakai H, Vreven T, Throssell K, Montgomery J A, Peralta Jr J E, Ogliaro F, Bearpark M J, Heyd J J, Brothers E N, Kudin K N, Staroverov V N, Keith T A, Kobayashi R, Normand J, Raghavachari K, Rendell A P, Burant J C, Iyengar S S, Tomasi J, Cossi M, Millam J M, Klene M, Adamo C, Cammi R, Ochterski J W, Martin R L, Morokuma K, Farkas O, Foresman J B & Fox D J, Gaussian, Inc., Wallingford CT, (2016).
20 O'Boyle N M, Tenderholt A L, Langner K M, *J Comp Chem*, 29 (2008) 839-845.
21 Avogadro: an open-source molecular builder and visualization tool. Version 1.1.0. http://avogadro.openmolecules.net/
22 Hanwell M D, Curtis D E, Lonie D C, Vandermeersch T, Zurek E & Hutchison G R, *J Cheminform* ,4 (2012) 17.